JCB Journal of Cell Biology

REPORT

Nuclear role for human Argonaute-1 as an estrogen-dependent transcription coactivator

Luciana I. Gómez Acuña[1], Ezequiel Nazer[1]*, Santiago A. Rodríguez-Seguí[1]*, Berta Pozzi[1], Valeria Buggiano[1], Luciano E. Marasco[1], Eneritz Agirre[2], Cody He[3], Mariano Alló[1], and Alberto R. Kornblihtt[1]

In mammals, argonaute (AGO) proteins have been characterized for their roles in small RNA–mediated posttranscriptional and also in transcriptional gene silencing. Here, we report a different role for AGO1 in estradiol-triggered transcriptional activation in human cells. We show that in MCF-7 mammary gland cells, AGO1 associates with transcriptional enhancers of estrogen receptor α (ERα) and that this association is up-regulated by treating the cells with estrogen (E2), displaying a positive correlation with the activation of these enhancers. Moreover, we show that AGO1 interacts with ERα and that this interaction is also increased by E2 treatment, but occurs in the absence of RNA. We show that AGO1 acts positively as a coactivator in estradiol-triggered transcription regulation by promoting ERα binding to its enhancers. Consistently, AGO1 depletion decreases long-range contacts between ERα enhancers and their target promoters. Our results point to a role of AGO1 in transcriptional regulation in human cells that is independent from small RNA binding.

Introduction

Argonaute (AGO) proteins are key players in the mechanisms of gene expression regulated by small noncoding RNAs (Meister, 2013). They have been well characterized as the effectors of siRNA- and miRNA-mediated posttranscriptional gene silencing (PTGS), a cytoplasmic process widely conserved along eukaryotes (Joshua-Tor and Hannon, 2011; Swarts et al., 2014). Briefly, different classes of small RNAs are able to interact with AGO proteins and, in such multimolecular complexes, to hybridize with target mRNAs via perfect or partial RNA:RNA sequence complementarity and to trigger mRNA endonucleolytic cleavage, translation inhibition, or mRNA degradation, depending on the degree of complementarity (Ipsaro and Joshua-Tor, 2015; Meister, 2013). In certain organisms, AGO proteins have also been reported as regulators of gene expression at the transcriptional level. For example, they are involved in siRNA-mediated transcriptional gene silencing (TGS) in *Schizosaccharomyces pombe*, where they are recruited to the pericentromeric repeats by perfect complementarity between the bound siRNAs and nascent transcripts to further recruit histone methyl transferases that induce heterochromatin formation (Holoch and Moazed, 2015). Interestingly, the heterochromatin-forming siRNAs are generated by processing of the transcripts generated at the same locus that is being silenced. In a similar way, AGO proteins are responsible for small RNA–mediated TGS in *Caenorhabditis elegans* (Guang et al., 2010; Guérin et al., 2014). In *Drosophila melanogaster*, however, AGO proteins were found to have a different and even opposite role: DmAGO2 is enriched at transcriptional active genomic loci, where it was found to interact with the transcriptional machinery regulating transcription by either releasing RNA polymerase II from promoter proximal pausing or by favoring enhancer–promoter chromatin loop formation (Cernilogar et al., 2011; Moshkovich et al., 2011). More recent evidence reinforces the idea that DmAGO2 modulates chromatin topology and gene expression in an RNAi-independent manner (Nazer et al., 2018b, 2018a).

While several efforts have been made to elucidate a possible role for AGO proteins in mammalian transcriptional regulation, the matter is far from being understood, mainly because the first reports addressing this issue used exogenous siRNAs that, when targeted to promoter regions, resulted in H3K9me2-dependent TGS (Han et al., 2007; Janowski et al., 2006; Morris et al., 2004). In addition to this, exogenous siRNAs targeted to promoters and regulatory regions have been shown to trigger transcriptional activation (Janowski et al., 2007; Li et al., 2016) and to affect alternative splicing decisions when targeted to introns through a TGS-like mechanism (Alló et al., 2009). However, despite

[1]Universidad de Buenos Aires, Facultad de Ciencias Exactas y Naturales, Departamento de Fisiología, Biología Molecular y Celular and Consejo Nacional de Investigaciones Científicas y Técnicas de Argentina, Instituto de Fisiología, Biología Molecular y Neurociencias, Buenos Aires, Argentina; [2]Karolinska Institutet, Stockholm, Sweden; [3]Pritzker School of Medicine, University of Chicago, Chicago, IL.

*E. Nazer and S.A. Rodríguez-Sequí contributed equally to this paper; Correspondence to Alberto R. Kornblihtt: ark@fbmc.fcen.uba.ar; Luciana I. Gómez Acuña's present address is Medical Research Council Human Genetics Unit, Institute of Genetics and Molecular Medicine, University of Edinburgh, Edinburgh, UK.

intense research, so far there is no evidence for endogenous siRNAs or miRNAs driving a TGS mechanism in mammalian cells.

In humans, four AGO proteins (AGO1–4) are expressed. From these, only AGO2 has the endonuclease activity required for cleavage of the target mRNA (Meister, 2013). Being partially redundant, they are all ubiquitously expressed, as it was shown that they have binding preferences within miRNA subpopulations (Burroughs et al., 2011). Although it was clearly shown that AGO proteins can be found in the nuclei of human cells (Ahlenstiel et al., 2012; Ameyar-Zazoua et al., 2012; Gagnon et al., 2014a), compared with their well-established cytoplasmic roles, much less is known about putative nuclear functions for AGO proteins in mammals. As a way of addressing this question, we previously analyzed the genome-wide distribution of AGO1 in human mammary gland tumor cells (MCF-7 cell line) and found that AGO1 preferentially binds transcriptional enhancers (Alló et al., 2014). The fact that AGO1 binding prevails in active enhancers, as revealed by the type and level of histone marks associated with them, raises the question of whether AGO1 is acting on transcription activation rather than in silencing. In an independent report, others have shown that human AGO1 associates with active promoters in human prostate tumor PC3 cells, interacting with the transcriptional machinery and acting in a positive way on transcription, whereas AGO2 showed no genomic enrichment at all in the same cell line (Huang et al., 2013). In contrast, it was also shown that AGO2 interacts with estrogen receptor β (ERβ) in human BC cells and that it is involved in ERβ-mediated regulation of transcription (Tarallo et al., 2017). More recently, human AGO1 was also shown to strongly associate with active transcriptional enhancers and nascent RNA generated at these sites, and its depletion led to changes in chromatin topology in HepG2 cells (Shuaib et al., 2019). The involvement of endogenous siRNAs in AGO1 recruitment to these enhancer or promoter regions is a matter that has not yet been resolved. These intriguing observations encouraged us to investigate the role of AGO1 in enhancer activation and in transcription regulation in MCF-7 cells.

Many transcriptional regulatory regions or enhancers are known to be located tens to hundreds of kilobases away from the promoter of the regulated genes (Vernimmen and Bickmore, 2015). Understanding the mechanisms by which they function and exert their influence over long stretches of genomic DNA is of paramount importance. ERα enhancers are a widely used model of signal-induced transcriptional activation. Upon estradiol (E2) treatment, rapid and transient transcriptional activation occurs in thousands of genes across the genome (Hah et al., 2011). Transcriptional activation is driven by a set of primed enhancers that become active upon ERα binding, in turn dependent on hormone binding, showing increased enhancer RNA (eRNA) levels and increased long-range interaction with their target genes (Hah et al., 2013; Hurtado et al., 2011; Li et al., 2013; Magnani and Lupien, 2014; Tan et al., 2011).

The evidence reported here further supports a nuclear function for AGO1 as a transcriptional coactivator. We show that in MCF-7 cells, AGO1 has a conspicuous nuclear localization and almost exclusively binds to estrogen-responsive enhancers genome wide and that this binding is enhanced by treatment of the cells with E2. Moreover, we demonstrate that AGO1 physically interacts with ERα and that this interaction is promoted by E2 but is insensitive to RNase treatment. Upon AGO1 knockdown, transcriptional activation of example genes controlled by E2 via their cognate ERα enhancers is largely impaired due to the fact that ERα recruitment to their enhancers and production of eRNAs are reduced. We also show that AGO1 depletion decreases long-range contacts between ERα enhancers and their target promoters. Furthermore, we show here that AGO1 binding to small RNAs is not needed for its role as a positive transcriptional activator.

Results and discussion

AGO1 locates at ERα binding sites

To assess the role of AGO1 in the activity of the regulatory regions to which it binds, we first decided to investigate whether AGO1 is enriched within specific sets of transcriptional regulatory regions in MCF-7 cells. To focus on bona fide AGO1 sites, we performed a new analysis of our published AGO1 chromatin immunoprecipitation (ChIP) sequencing (ChIP-seq) data (Alló et al., 2014) of MCF-7 cells with more stringent thresholds (see Materials and methods). In these conditions, we detected 2,871 AGO1 binding sites. As a first exploratory approach, we performed a de novo motif analysis at these AGO1-enriched regions (Fig. 1 A). Binding motifs for numerous transcription factors (TFs) were found to be enriched at these sites, being that the ERα motif is the one recovered with the lowest P value (1e−134), which was 75 orders of magnitude smaller than the second-best match (MYBL2-like; P = 1e−59). In a subsequent analysis, the enrichment of known binding motifs for TFs expressed in MCF-7 cells was assessed. Consistent with the de novo analysis, this also revealed that AGO1 regions are enriched in the ERα binding motif: the P value with which this motif is recovered (1e−149) is again strikingly lower than the second-best match (ESRRB; P = 1e−11) included in this analysis (Fig. S1 A). Among the other motifs recovered, it is worth noting those for FOXA1, a pioneer TF known to be involved in ERα enhancer priming (Magnani and Lupien, 2014), and for AP2 TFs, also known to be involved in ERα-mediated transcriptional activation by assisting ERα indirect binding to some of the enhancers (Tan et al., 2011).

To further study the nature of AGO1-enriched regions, we used available ChIP-seq data of several TFs obtained from MCF-7 cells (Table S1). MCF-7 datasets include ERα ChIP-seq upon estradiol treatment (+E2), FOXA1 ChIP-seq, and progesterone receptor (PR) ChIP-seq upon progestogen treatment. Both ERα and PR belong to the family of nuclear receptors, and their binding sites across the genome are known to partially overlap. We found that AGO1-enriched regions are also significantly enriched in these TFs in MCF-7 cells (Fig. S1 B), being that ERα is the one with the highest region overlap fold of enrichment.

Since the motif analysis revealed clear enrichment of the ERα binding motif at AGO1 binding sites, we decided to test whether the observed TF enrichment at AGO1-binding regions depended on ERα cobinding. We divided the peaks of the different TFs included in the previous analysis into bins, depending on whether they occupied ERα binding regions (ERα$^+$) or not

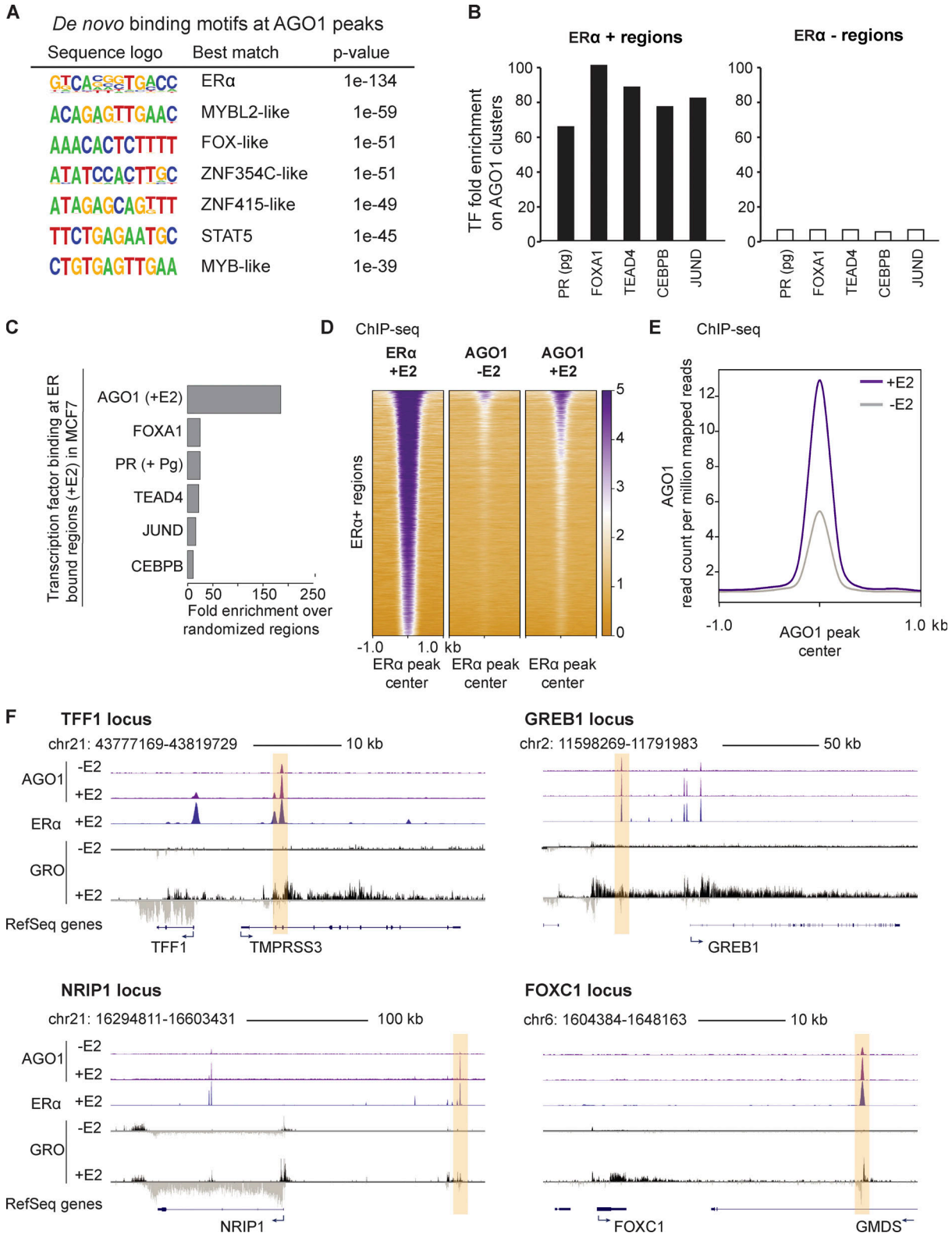

Figure 1. **AGO1 locates at ERα binding sites, and its binding is enhanced by E2. (A)** De novo DNA motif analysis at AGO1-associated genomic regions. **(B)** Enrichment of TF binding at AGO1-associated regions in serum-maintained MCF-7 cells, divided according to whether they are also bound by ERα (left panel) or not (right panel). ChIP-seq peak overlaps are shown for AGO1(1), PR (2), FOXA1 (2), TEAD4 (1), CEBPB (1), and JUND (1), where the number of replicates is shown between parentheses. **(C)** TF overlap with ERα-bound regions (in E2-treated cells), expressed as fold enrichment over randomized regions. **(D)** Heat maps of ChIP-seq signal centered (±1 kb) on ERα binding site midpoints for ERα (+E2), AGO1 (−E2), and AGO1 (+E2) regions. Regions are ordered from high to low ERα signal. **(E)** AGO1 reads per million mapped reads (RPM) around (±1 kb). AGO1 binding sites are defined by pooling AGO1 peaks from both treatments (−E2 and +E2). **(F)** UCSC genome browser screenshots showing four loci comprising ERα enhancers and neighboring genes that are up-regulated upon E2 treatment. Tracks correspond to RefSeq genes, AGO1 ChIP-seq, ERα (+E2) ChIP-seq, and GRO-seq plus and minus strands −E2 and +E2, all from MCF-7 cells.

(ERα⁻). Strikingly, only the TF binding sites that occupied ERα⁺ regions were enriched at AGO1 binding sites (Fig. 1 B). Those TF-enriched regions that did not coincide with ERα had no overlap with AGO1. We conclude then that while AGO1-enriched regions may overlap with several TF binding regions, this is dependent on their capacity to be associated with the ERα.

AGO1 binding to ERα target sites increases upon estradiol (E2) treatment without changes in its subcellular localization

It is well established that ERα binds primed transcriptional enhancers in an E2-dependent manner (Hah et al., 2011; Hurtado et al., 2011; Magnani and Lupien, 2014). Upon hormone treatment, ERα translocates from the cytoplasm to the nucleus, where it dimerizes and binds the transcriptional regulatory regions already bound by pioneer and other TFs (Renoir, 2012).

Due to the observation that AGO1 is enriched in ERα binding sites when MCF-7 cells are cultured with normal serum (Fig. 1, A and B; and Fig. S1, A and B), we decided to perform new AGO1 ChIP-seq experiments in MCF-7 cells starved (−E2) or treated with E2 (+E2), following the protocol depicted in Fig. S1 C. The AGO1 ChIP signal was analyzed relative to input, and this was contrasted with known hyper-ChIPable hotspots to discard artifactual enrichment (Teytelman et al., 2013). More than 90% of AGO1 ChIP-seq peaks were found at ERα binding sites in either condition (Fig. S1 D). When normalized read densities were considered over identified peaks, samples clustered well on the basis of replicates in contrast to E2 treatment (Fig. S1 E). AGO1 enrichment on ERα binding sites upon E2 treatment was clearly higher than any other TF analyzed (Fig. 1 C). Although AGO1 was also detected bound to chromatin on ERα sites in untreated cells, AGO1 read density clearly increased in E2-treated MCF-7 cells (Fig. 1 D). An additional analysis shows that most AGO1 binding sites gained binding affinity in E2-treated cells (Fig. S1 F). When total AGO1 peaks found in both conditions were analyzed, the average AGO1 ChIP signal was also higher in E2-treated cells than in untreated cells (Fig. 1 E). We concluded then that AGO1 binding to ERα target sites increases with E2 in MCF-7 cells.

Fig. 1 F shows four examples of genome browser snapshots for the *TFF1*, *GREB1*, *NRIP1*, and *FOXC1* loci, illustrating the strong correlation between AGO1 and ERα binding to chromatin. AGO1 E2-dependent enrichment on the highlighted regions was confirmed by ChIP–quantitative PCR (qPCR), where ERα levels were also assessed (Fig. S1, G and H). Additionally, an increase in AGO1 in chromatin binding cannot be explained by an increase in AGO1 total levels, as analyzed by Western blot (Fig. S2 A).

We next sought to determine if AGO1 binding to ERα target sites follows changes in its subcellular localization. While the amount of ERα observed in nuclear extracts by Western blot clearly increased in detriment to the amount in the cytoplasmic extracts when cells were treated with E2, AGO1 distribution between cytoplasmic and nuclear extracts remained unchanged (Fig. S2 B). This was also corroborated by AGO1 immunofluorescent staining in fixed MCF-7 cells followed by confocal microscopy (Fig. S2, C and D). AGO1 is found in both the nucleus and the cytoplasm, and its distribution between these compartments is similar in hormone-depleted and E2-treated cells. We conclude that AGO1 displays a conspicuous nuclear localization and that the increase in AGO1 binding to ERα binding sites upon hormonal treatment is not due to an up-regulation of its translocation to the nucleus.

AGO1 knockdown impairs E2-dependent ERα binding to chromatin

A large proportion of AGO1 peaks of E2-treated cells overlaps with ERα, but only a small proportion of ERα peaks overlaps with AGO1. For further analysis, we divided ERα peaks according to whether they overlap with AGO1 (ERα⁺/AGO1⁺) or not (ERα⁺/AGO1⁻). In light of the mechanistic evidence supporting nuclear roles of AGO2 in *D. melanogaster* (Cernilogar et al., 2011; Guang et al., 2010; Moshkovich et al., 2011; Taliaferro et al., 2013), we decided to further investigate whether AGO1 binding to a certain fraction of ERα sites correlates with other features, such as those included in the so-called CTCF chromatin states (Taberlay et al., 2014). Fig. S3 A shows that, although enrichment is very low and is similar for both ER subsets in CTCF-only chromatin, both ERα⁺/AGO1⁺ and ERα⁺/AGO1⁻ regions are more enriched in CTCF⁺Enhancer⁻ and CTCF⁺Promoter⁻ chromatin states, with higher enrichment for ERα⁺/AGO1⁺. We then analyzed the E2-dependent ERα normalized read counts in both groups (Fig. 2 A). ERα normalized read counts were clearly higher on ERα⁺/AGO1⁺ (1,935 regions) compared with ERα⁺/AGO1⁻ (6,796 regions). ERα normalized read densities on these two groups of regions are also shown (Fig. S3 B).

To test whether ERα binding to chromatin upon E2 treatment depends on AGO1 cobinding, we transiently knocked down AGO1 by transfecting MCF-7 cells with specific siRNAs. Knockdown efficiency was tested both by total protein Western blot (Fig. 2 B) and by AGO1 ChIP-qPCR enrichment analysis on the ERα enhancers depicted in Fig. 1 F (Fig. S3 C). It is worth noting that depletion of AGO1 did not affect ERα total levels (Fig. 2 B). AGO1 knockdown decreased E2-dependent binding of ERα to the ERα⁺/AGO1⁺ sites depicted in Fig. 1 F (Fig. 2 C), which indicates that AGO1 is involved in the first steps of ERα enhancer activation after hormone treatment. It is worth noting that the reduction of ERα levels upon E2 and AGO1 knockdown was not total (i.e., levels were not reduced to the basal levels without E2). This could be explained by the fact that AGO1 knockdown was not total (Fig. 2 B). Alternatively, we cannot exclude that other AGO proteins are also involved in ERα enhancer function. Further analysis revealed that AGO1 knockdown also affects ERα E2-dependent recruitment to ERα⁺/AGO1⁻ regions (Fig. 2 D). Considering then that a small subset of ERα peaks is cobound with AGO1 but that all of the ERα peaks analyzed here (both AGO1⁺ and AGO1⁻) show decreased binding levels upon AGO1 knockdown, we conclude that the latter can be explained by a low AGO1 ChIP efficiency. AGO1 could be recruited at a lower intensity to far more ERα regions upon E2 treatment than the ones detected here.

AGO1 interacts with ERα in an E2-dependent manner

ERα and AGO1 display similar behaviors in their E2-dependent binding to chromatin (Fig. 1 D and Fig. 2, C and D). To test whether AGO1 interacts with ERα directly or within the same protein complex, we immunoprecipitated endogenous AGO1

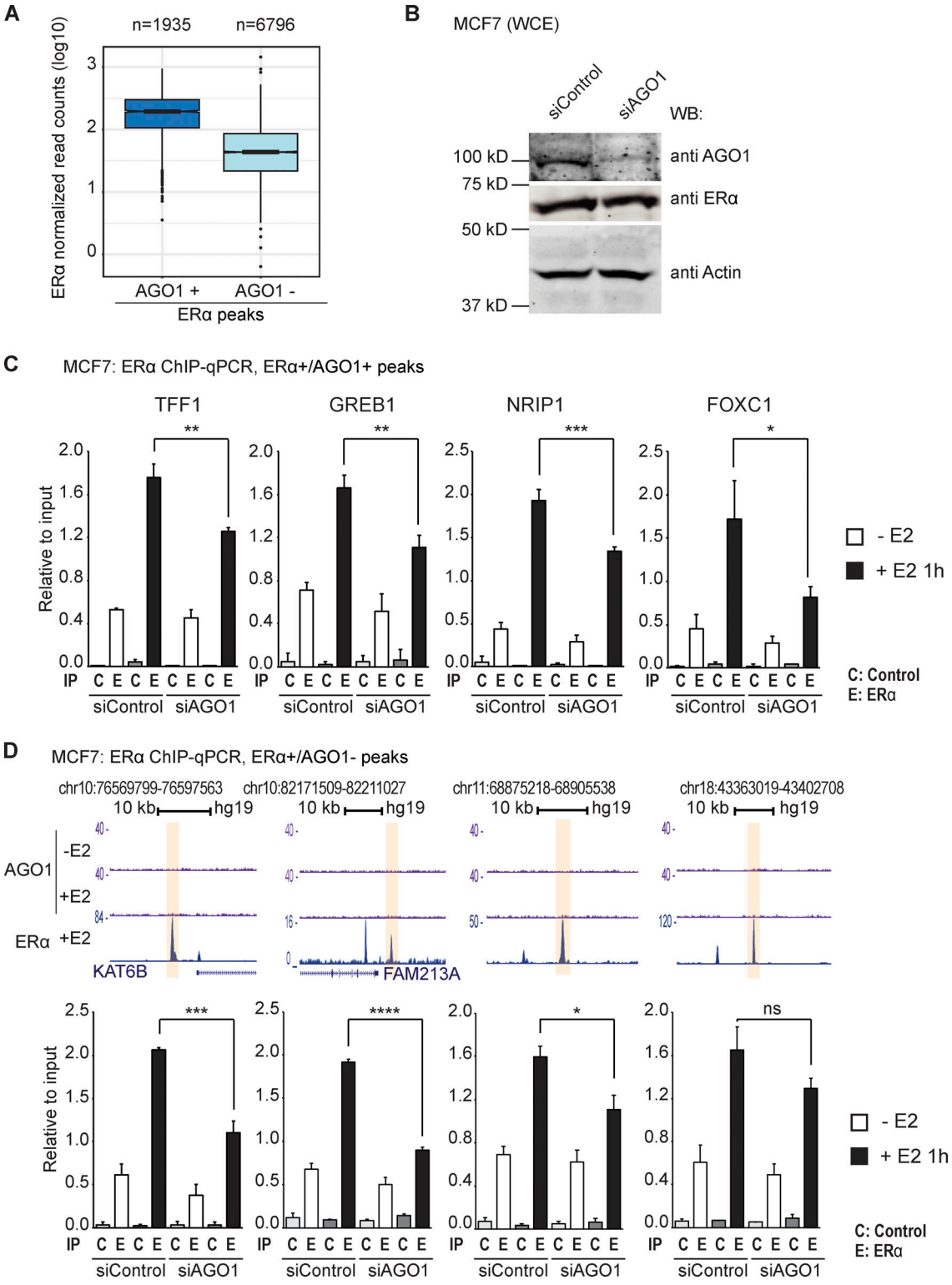

Figure 2. **ERα binding to chromatin depends on AGO1. (A)** ERα (+E2) ChIP-seq normalized read counts over ERα⁺/AGO1⁺ and ERα⁺/AGO1⁻ regions. **(B–D)** MCF-7 cells were transfected with an siControl or siAGO1. 24 h later, they were hormone starved, and 72 h later, they were treated with E2 or vehicle for 1 h. **(B)** AGO1 knockdown efficiency was tested by Western blot (WB) from whole-cell extracts (WCE). **(C)** E2-dependent ERα recruitment to ERα⁺/AGO1⁺ regions was analyzed by ChIP-qPCR. **(D)** E2-dependent ERα recruitment to ERα⁺/AGO1⁻ regions was analyzed by ChIP-qPCR. Values in C and D represent mean ± SE with $n = 3$ (i.e., three independent experiments). *, $P < 0.05$; **, $P < 0.01$; ***, $P < 0.001$; ****, $P < 0.0001$; ANOVA and Tukey post-hoc test. ns, not significant; IP, immunoprecipitation.

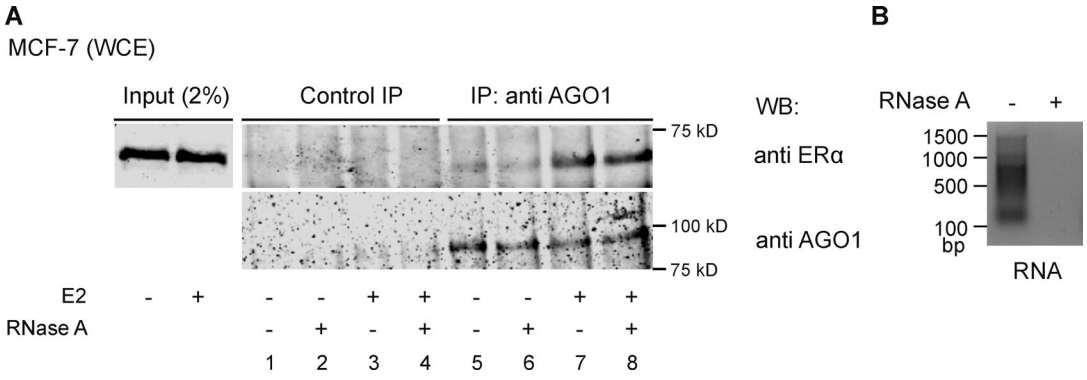

Figure 3. **AGO1 physically interacts with ERα in an E2-dependent and RNA-independent manner. (A)** MCF-7 cells were hormone starved and treated with vehicle or E2 for 1 h. Whole-cell extracts (WCE) were treated or not with RNase A, and then they were immunoprecipitated (IP) with control or anti-AGO1 antibody. AGO1 and ERα presence in inputs and immunoprecipitates was analyzed by Western blot (WB). **(B)** Representative agarose gel showing RNase treatment efficiency.

from MCF-7 whole-cell extracts and analyzed the presence of endogenous ERα in the immunoprecipitate (coimmunoprecipitation assay). ERα immunoprecipitates when the extracts are incubated with an anti-AGO1 antibody and not with a control antibody (Fig. 3 A). Moreover, the efficiency of bringing down ERα with the anti-AGO1 antibody is higher when treating MCF-7 cells with E2 compared with hormone-starved cells (Fig. 3 A; compare lanes 1, 3, 5, and 7). As coimmunoprecipitation assays were performed with whole-cell extracts as starting material, it is unlikely that the differential coimmunoprecipitation observed with E2 was due to the different compartmentalization observed in Fig. S2 D. ERα is subjected to many posttranslational modifications upon ligand binding (Le Romancer et al., 2011), allowing us to speculate that this result might be due to AGO1 interacting directly or indirectly to ERα harboring specific posttranslational modifications.

AGO1 association with chromatin correlates with eRNA expression

We next decided to investigate whether AGO1 is associated with enhancer activation. In the previous report (Alló et al., 2014), we showed that AGO1 is preferentially enriched at active transcriptional enhancers, as revealed by the nature and level of the histone marks typically associated with active enhancers. Accordingly, when comparing ERα binding sites that are also bound by AGO1 ($ERα^+/AGO1^+$; 1,935 regions) with those that are not ($ERα^+/AGO1^-$; 6,796 regions), we observed that +E2/−E2 fold change in eRNA levels was higher in $ERα^+/AGO1^+$ than in $ERα^+/AGO1^-$ (Fig. 4 A). Considering that enhancer transcription into eRNAs is the best marker for enhancer activation (Hah et al., 2013; Li et al., 2013), we conclude that AGO1 enrichment on ERα enhancer positively correlates with enhancer activation levels.

AGO1 is necessary for the transcriptional activation by E2 of genes controlled by ERα enhancers

The above-demonstrated interaction between AGO1, ERα, and ERα enhancers, although specific, could be a circumstantial event without further relevant biological implications. The fact that these interactions do not require the participation of small RNAs, or in fact any kind of RNA (Fig. 3 A), suggests that if a function exists, this must be novel and unrelated to both PTGS and TGS. We then sought to determine if AGO1 is necessary for the transcriptional activation of the ERα enhancers. We based this analysis on the four previously chosen loci (Fig. 1 F) in which GRO-seq tracks (Li et al., 2013) showed eRNA up-regulation at the ERα enhancers upon E2 treatment. The tracks also showed the E2-dependent transcriptional activation of their neighboring genes (*TFF1*, *GREB1*, *NRIP1*, and *FOXC1*), which we will consider as targets (Li et al., 2013). We first analyzed the eRNA levels generated from the ERα enhancers in cells subjected to AGO1 knockdown and E2 treatment for 1 h by reverse transcriptase qPCR (RT-qPCR). AGO1 knockdown efficiency was assessed here by RT-qPCR (Fig. 4 B). AGO1 knockdown abolishes the up-regulation of enhancer transcription (Fig. 4 C) consistently, with the idea that ERα enhancer activation is dependent on AGO1. Accordingly, transcriptional activation of the target genes is greatly inhibited by AGO1 depletion, both at the pre-mRNA (Fig. 4 D) and the mature mRNA (Fig. S3 D) levels. No changes in pre-mRNA levels were observed in the case of non–E2-regulated genes (Fig. 4 E), pointing to a specific role of AGO1 in ERα-regulated gene expression in MCF-7 cells, although genome-wide expression studies are lacking at this point. Similar effects are observed in independent experiments in which a different siRNA to AGO1 mRNA was transfected (Fig. S3 E), arguing against possible off-target artifacts.

As a first step to understand the role of AGO1 in transcription of genes regulated by ERα enhancers, we performed chromosome conformation capture (3C) at three different loci (corresponding to the E2-regulated genes *NRIP1*, *TFF1*, and *GREB1*) and found that the long-range interaction observed between the ERα enhancers and the promoter regions of their target genes were reduced upon AGO1 knockdown (Fig. 4 F). No significant reduction was observed in the interactions between the *FOS1* gene promoter and its closest ERα binding site that does not bind AGO1 and between the *FOS1* gene promoter and a negative control region (Fig. 4 G). Finally, as an additional negative control, no changes in the interaction between the non–E2-

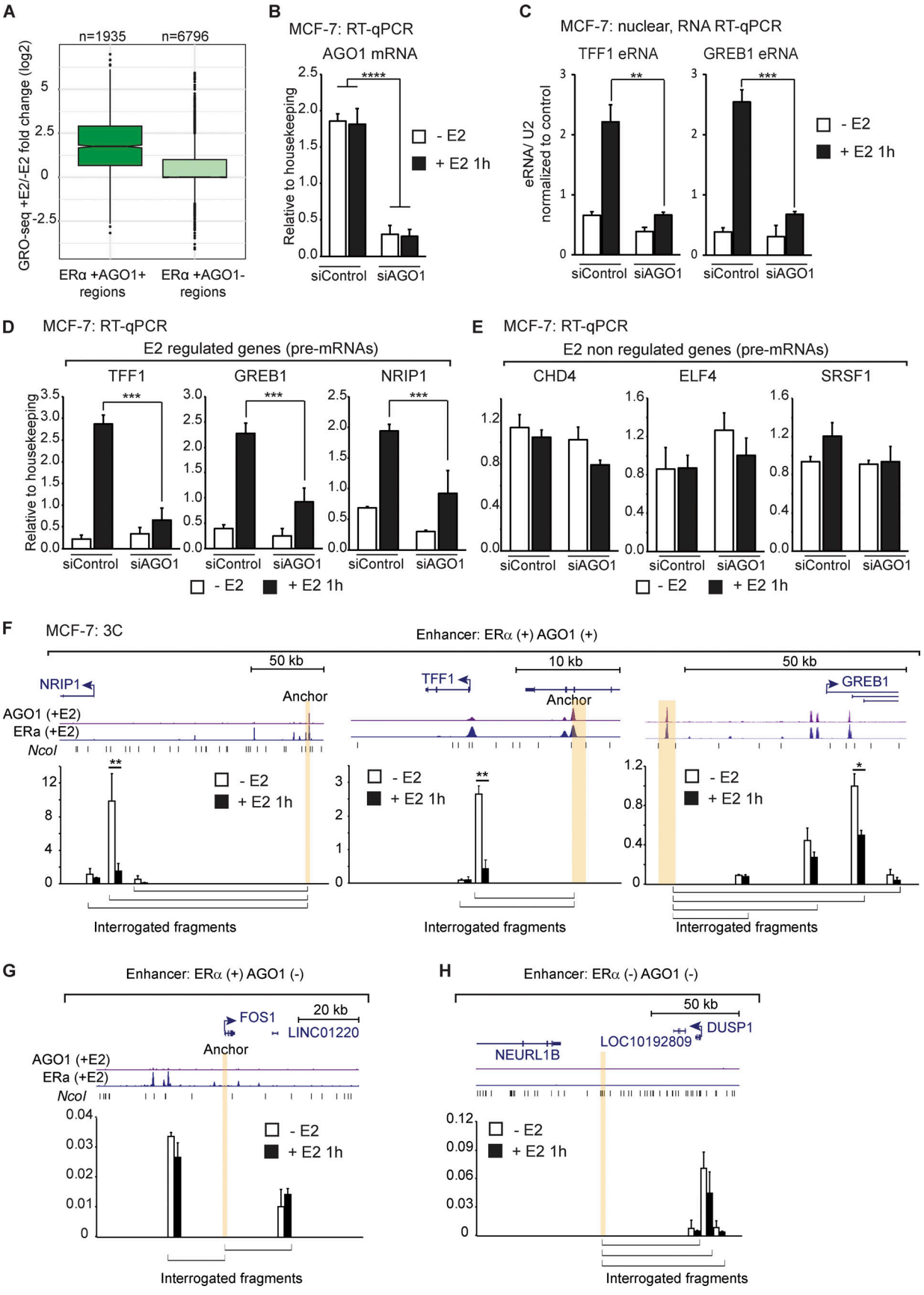

Figure 4. **AGO1 participates in the transcriptional activation of E2-responsive genes controlled by ERα enhancers by promoting three steps of ERα enhancer activation. (A)** GRO-seq read count fold change between −E2 and +E2 treatments over ERα⁺/AGO1⁺ and ERα⁺/AGO1⁻ regions. **(B–H)** MCF-7 cells

were transfected with an siControl or siAGO1. 24 h later, they were hormone starved, and 72 h later, they were treated with E2 or vehicle for 1 h. **(B)** Total RNA was extracted, and AGO1 knockdown was assessed by RT-qPCR. **(C)** Nuclear RNA was extracted, and the indicated eRNA levels were analyzed by RT-qPCR. **(D)** Total RNA was extracted, and the indicated pre-mRNA levels corresponding to E2-regulated genes were analyzed by RT-qPCR. **(E)** Total RNA was extracted, and the indicated pre-mRNA levels corresponding to non–E2-regulated genes were analyzed by RT-qPCR. **(F)** Frequency of chromatin loops formation between the indicated restriction fragments was analyzed by 3C. The anchor region, with which all of the interactions were tested, comprises an ERα$^+$/AGO1$^+$ region. AGO1 ChIP-seq and ERα ChIP-seq tracks are shown along the position of the proximal E2-regulated genes. **(G)** Same as F, but here the anchor region comprises an ERα$^+$/AGO1$^-$ region. **(H)** Same as G, but here the anchor region comprises a non–E2-regulated enhancer region. Values in B–E represent mean ± SE from three independent experiments (**, P < 0.01; ***, P < 0.001; ****, P < 0.0001; ANOVA and Tukey post-hoc test). Values in F–H represent mean ± SE from three independent experiments (*, P < 0.05; **, P < 0.01; two-tailed Student's *t* test).

regulated gene *DUSP1* and its enhancer (not bound by ERα) were observed (Fig. 4 H).

AGO1 functional role at ERα transcriptional enhancers does not depend on small RNA binding

AGO proteins bind small RNAs and are widely known to interact with mRNAs through RNA:RNA complementarity. The above-reported AGO1 and ERα interaction, however, was not affected upon treatment of MCF-7 whole-cell extracts with RNase A before and during incubations with the specific and control antibodies (Fig. 3 A, lanes 3, 4, 7, and 8). To further explore a putative role of small RNAs in AGO1 function at ERα transcriptional enhancers, we decided to use an AGO1 mutant that fails to bind small RNAs (Faehnle et al., 2013; Rüdel et al., 2011; Fig. 5 A). This AGO1 mutant bears a phospho-mimetic point mutation at the MID domain (Y527E) that impairs binding to the 5′ overhang of the small RNAs (Faehnle et al., 2013; Rüdel et al., 2011). AGO1 was knocked down in MCF-7 cells using siRNAs, and rescue of AGO1 loss of function was attempted by expression of adenoviral vectors encoding GFP, AGO1 WT, or AGO1 Y527E. As shown in Fig. 5 B, AGO1 knockdown efficiency is high, and rescue protein levels with the exogenous constructs are similar to the endogenous (siRNA control [siControl] + GFP) ones. As observed in Fig. 2 C, expression of the E2-regulated genes TFF1 and GREB1, measured at the pre-mRNA level, is reduced upon AGO1 knockdown, and expression levels are reestablished when rescuing AGO1 expression with either the WT or the Y527E mutant constructs (Fig. 5 C). eRNA levels of the *FOS1* E2-regulated enhancer (corresponding to an ERα$^+$/AGO1$^-$ region) are not changed by knocking down AGO1 or rescuing its expression with either construct, although the same trend is observed (Fig. 5 D). In line with reports highlighting small RNA–independent nuclear roles of AGO proteins in *D. melanogaster* (Zaytseva et al., 2020 *Preprint*), the evidence reported here points us to a positive role of AGO1 in E2-regulated gene expression that does not depend on small RNA binding and small RNA--RNA interactions.

Many proteins are found, named, and characterized for a particular function to later discover that they participate in cell processes that are completely different from those of the original findings. This seems to be the case with human AGO1, a protein primarily characterized as a key factor in cytoplasmic PTGS and with some evidence for roles in nuclear TGS. We uncovered here a role for AGO1 in estradiol-triggered transcriptional activation in human cells. Following our previous findings that AGO1 binds transcriptional regulatory regions preferentially when active, we show here that in the tumor-derived MCF-7 mammary gland cells, AGO1 associates with ERα transcriptional enhancers and that this association is up-regulated by treating the cells with E2, which displays a positive correlation with the activation level of these enhancers. Moreover, we show that AGO1 physically interacts with ERα either directly or in the same protein complex, and again, this interaction is increased by E2 treatment. Furthermore, the interaction occurred in the absence of RNA. While ERα translocates to the nucleus upon E2 treatment, we demonstrated that the nucleo/cytoplasmic distribution of AGO1 was quantitatively similar in both untreated and E2-treated cells. This evidence suggests that the ERα/AGO1 interaction occurs when both proteins are bound to chromatin. Most importantly, our analysis of a few, well-characterized, E2-regulated loci supports the notion that AGO1 acts positively in estradiol-triggered transcriptional activation: AGO1 knockdown reduced (i) ERα binding to the enhancers, (ii) the transcriptional activation level of the target genes, and (iii) the long-range interaction between enhancers and their target gene promoter. In addition, we show that the inhibition of E2-dependent transcriptional activation of the studied target genes by AGO1 knockdown can be equally rescued by both WT AGO1 and the Y527E mutant, unable to bind to the 5′ overhang of small RNAs. This provides further evidence that RNA binding is dispensable for the new role of AGO1 reported here.

Based on the above evidence and the lack of a DNA-binding domain, we wish to propose that AGO1 is a transcriptional coactivator, since it fits the textbook definition of "a protein that does not itself bind DNA but assembles on other DNA-bound gene regulatory proteins to activate transcription of a gene" (Alberts et al., 2015). More specifically, because of its interaction with a nuclear receptor (ERα) and results in Fig. 4, AGO1 perfectly fits the definition of a nuclear receptor coregulator (i.e., a cellular factor recruited by nuclear receptors that complements their function as mediators of the cellular response to endocrine signals; McKenna and O'Malley, 2002). Coregulators include coactivators and corepressors. One may wonder whether AGO1 also acts as a corepressor of certain genes. Indeed, steroid hormone receptors are able to repress transcription by inducing chromatin compaction around the transcription start sites of target genes in a mechanism that involves HP1γ-LSD1 repressor complex recruitment to the promoter regions (Nacht et al., 2016). Repression acts, however, at the level of gene promoters and not at distal enhancers, which seems unlikely for AGO1 in light of the evidence reported here.

Due to concerns about the specificity of AGO1 antibodies, we previously validated the one used here (4B8) exhaustedly (Sigma-Aldrich; Alló et al., 2014). Additionally, we can argue

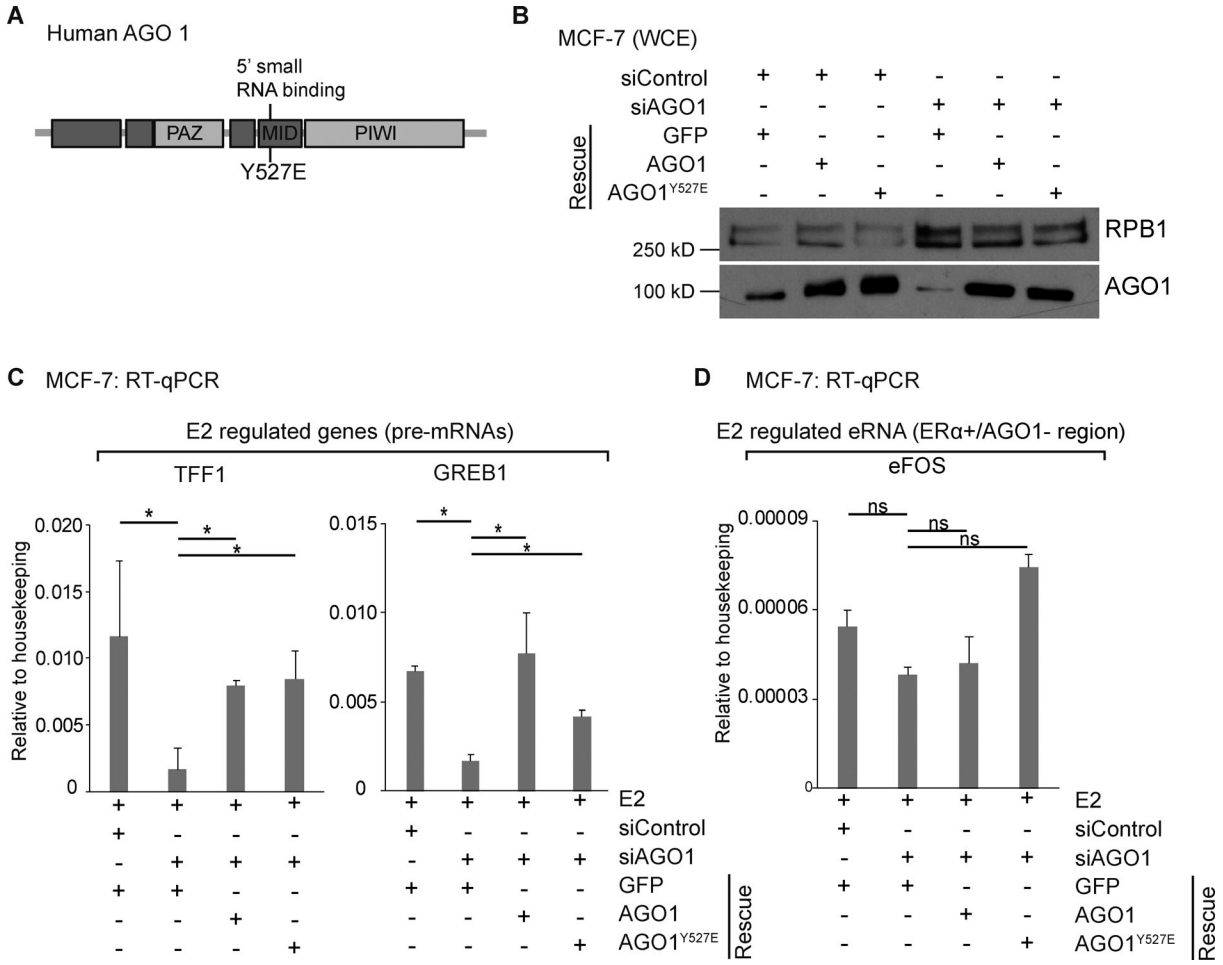

Figure 5. **AGO1 functional role at ERα transcriptional enhancers does not depend on small RNA binding. (A)** Schematic representation of AGO1 protein domains showing the position of the point mutation in the MID domain that impairs small RNA binding. **(B–D)** MCF-7 cells were transfected with the indicated siRNAs, and AGO1 expression was rescued by the indicated constructs before hormone starvation and E2 treatment. **(B)** AGO1 knockdown and rescue levels were assessed by Western blot. RPB1 corresponds to the housekeeping control. **(C)** The levels of the indicated pre-mRNA corresponding to E2-regulated genes were assessed by RT-qPCR. **(D)** The levels of the indicated eRNA corresponding to an E2-regulated eRNA were assessed by RT-qPCR. Values in C and D represent mean ± SE from three independent experiments (*, $P < 0.05$; two-tailed Student's *t* test). ns, not significant; WCE, whole-cell extracts.

against a putative cross reactivity with another protein of the AGO1 4B8 antibody used in our ChIP and coimmunoprecipitation assays. First, two different siRNAs targeting AGO1 mRNA are capable of reducing AGO1 levels detected by Western blotting using the same antibody used in our ChIP experiments. Second, AGO1 ChIP-qPCR enrichment levels are also reduced when specifically knocking down AGO1.

The role of AGO1 in transcriptional activation described here in human cells resembles the one found in *D. melanogaster*, whereby DmAGO2 binds transcriptionally active genomic regions either by interacting with the transcriptional machinery (Cernilogar et al., 2011; Nazer et al., 2018b) or by acting in transcriptional regulation by modulating chromatin topology (Moshkovich et al., 2011; Nazer et al., 2018a). Our findings do not contradict previous evidence showing that exogenous siRNAs targeted to genomic regions (promoters and introns) induce local heterochromatin formation (Alló et al., 2009; Han et al., 2007; Janowski et al., 2006; Morris et al., 2004). While the generation of endogenous siRNAs in mammalian cells is a matter of controversy (Gantier and Williams, 2007; Svoboda, 2014; Tam et al., 2008), it is conceivable that when siRNAs are provided exogenously, AGO1 and other components of the nuclear RNAi machinery are capable of performing TGS. In this context, our results are consistent with the observation that transfection of siRNAs targeted to promoter regions can induce transcriptional activation (Janowski et al., 2007; Li et al., 2016), probably helped by AGO proteins.

We found here a strong association between AGO1 and ERα enhancers in MCF-7 cells. We wonder, however, whether AGO1 activity on transcriptional enhancers is restricted to ERα enhancers alone or whether it can also be extended to hormone-responsive enhancers in general or to other signal-dependent or developmental enhancers. AGO1 was also reported to bind actively transcribed loci genome wide in HepG2 and K562 cells, contributing to global 3D genome architecture (Huang et al., 2013; Shuaib et al., 2019; Xiao et al., 2019). It was also reported that human AGO2 interacts with ERβ (Tarallo et al., 2017), which shares high sequence identity with ERα. All together, these and

our results reveal that AGO proteins play crucial roles in hormone-induced transcriptional activation. In a broader scenario, our findings fit with the fact that in a comprehensive study, many RNA-binding proteins were found to bind chromatin and to regulate transcription (Xiao et al., 2019).

Materials and methods

Cell culture and treatment

MCF-7 breast cancer cells were routinely grown in DMEM/nutrient mixture F-12 supplemented with 10% FBS and 100 µg/ml of Primocin (InvivoGen), which is active against bacteria, mycoplasma, and fungi. Cells were routinely checked for mycoplasma infection. For the experiments, cells were plated in the same media at a density of 2 × 10^5 cells in 12-well plates, and for 24 h, they were hormone starved by washing them thoroughly with PBS, adding DMEM/F-12 media without phenol red, and supplementing with 2% dextran-coated, charcoal-treated FBS. 72 h later, cells were treated with β-estradiol (E2, E8875; Sigma-Aldrich) or vehicle for the indicated time and harvested for downstream applications.

HEK293 cells were routinely grown in DMEM supplemented with 10% FBS, 100 U/ml of penicillin, and 100 µg/ml of streptomycin.

siRNA transfection

For knockdown experiments, siRNA transfections were performed 24 h after cells were plated using 3 µl of Lipofectamine 2000 (Thermo Fisher Scientific) per well of 12-well plates and siRNAs at a concentration of 25 nM. Cells were hormone starved 24 h after transfection as indicated before. 72 h later, cells were treated with β-estradiol or vehicle for the indicated time and harvested for downstream applications. Thermo Fisher Scientific Block-iT siRNAs with the following sequences were used: siControl, 5′-CUUACGCUGAGUACUUCGAdTdT-3′; siAGO1, 5′-GAGAAGAGGUGCUCAAGAAdTdT-3′; and siAGO1_2, 5′-AAACCCAAACCUAACCAGCdTdT-3′.

Plasmid transduction

For knockdown and rescue experiments, plasmids harboring different DNA constructs were packed into lentivirus and transduced into MCF-7 cells. For lentivirus production, HEK293 cells were used. Briefly, 4.5 × 10^6 HEK293 cells were seeded on a 10-cm dish 24 h before transfection. 1 h before transfection, medium was replaced with DMEM containing 10% FCS and 25 µM chloroquine. The following transfection mix was prepared, vortexed, let stand for 15 min at room temperature, and added to the cells: 1 ml DMEM (no FCS and no antibiotics), 1.6 µg pMD2.G (VSV-G viral envelope; Addgene plasmid 12259), 3.2 µg pCMVdR8.74 (packaging construct; Addgene plasmid 22036), 6.5 µg of the viral transfer plasmid, and 4 µg of polyethylenimine per microgram of DNA used. 6 h after transfection, medium was replaced with 8 ml of fresh DMEM containing 10% FCS. 48 h after transfection, 8 ml of culture medium containing the lentiviral particles was removed, and Polybrene at an 8-µg/ml final concentration was added. Aliquots were prepared and used immediately or stored at −80°C.

For knockdown and rescue experiments, 8 × 10^5 MCF-7 cells were seeded in 6-cm dishes and transfected with siRNAs as specified before. 24 h after siRNA transfection, cells were infected with the lentivirus prepared before. 1 h before infection, the medium was replaced with fresh medium containing 8 µg/ml Polybrene. The medium was then replaced with the medium containing the lentiviral particles at a 1:2 dilution if used fresh or nondiluted if used from the −80°C stock. 24 h after infection, cells were hormone starved as indicated before. 72 h later, cells were treated with β-estradiol or vehicle for the indicated time and harvested for downstream applications.

Plasmid constructions

The lentiviral vector driving expression of FLAG/HA-Ago1 (human) from the Syn promoter (pLV-FLAG-HA_Ago1) was generated by amplifying FLAG/HA-Ago1 from pIRESneo-FLAG/HA Ago1 (Addgene plasmid 10822). Site-directed mutagenesis was performed by the DpnI method, based on Stratagene's QuikChange specifications. The primers used to mutate Y 527 into E are forward, 5′-ACGTTTCACCTCAGCCTCCACCGGCGTCTTCCC-3′; and reverse, 5′-GGGAAGACGCCGGTGGAGGCTGAGGTGAAACGT-3′.

ChIP assay

Approximately 1–2 × 10^7 MCF-7 cells were cross-linked for 10 min in 1% formaldehyde in PBS at room temperature. Cross-linking reaction was stopped with glycine at a final concentration of 125 mM. Cells were washed twice with cold PBS and swelled on ice for 10 min in 5 mM Pipes, pH 8, 85 mM KCl, 0.5% Igepal CA630, and 1× protease inhibitor cocktail (Roche). Following centrifugation, the pellet enriched in nuclei was resuspended in 0.5 ml sonication buffer (50 mM Tris-HCl, pH 8.1, 1% SDS, and 10 mM EDTA, pH 8). DNA was sonicated in an ultrasonic bath (Bioruptor Diagenode) to an average length of 200–500 bp, and samples were centrifuged at 15,000 *g*. 20–40 µg of DNA was used in each immunoprecipitation, diluting chromatin at least 10 times in 1 ml immunoprecipitation buffer (15 mM Tris-HCl, pH 8.1, 1% Triton X-100, 1 mM EDTA, pH 8, 150 mM NaCl, and 1× protease inhibitor cocktail). Chromatin was immunoprecipitated overnight with 40 µl of protein G magnetic beads (Dynabeads Protein G; Thermo Fisher Scientific) previously incubated with the antibody of interest for 1 h at 4°C. The following antibodies were used: 5 µg of rat monoclonal anti-AGO1 clone 4B8 and 2 µg of rabbit polyclonal anti-ERα HC-20 (Santa Cruz Biotechnology). Control immunoprecipitations were performed with no antibody. Beads were washed sequentially for 5 min each in low-salt (20 mM Tris-HCl, pH 8, 150 mM NaCl, 2 mM EDTA, 1% Triton X-100, and 0.1% SDS), high-salt (20 mM Tris-HCl, pH 8, 500 mM NaCl, 2 mM EDTA, 1% Triton X-100, and 0.1% SDS), and LiCl buffer (10 mM Tris, pH 8.0, 1 mM EDTA, 250 mM LiCl, 1% Igepal CA630, and 1% sodium deoxycholate) for 5 min at 4°C and then twice in 1× Tris-EDTA (TE) for 5 min at room temperature. Beads were eluted in 1% SDS and 100 mM $NaHCO_3$ buffer for 1 h at room temperature, and cross-linking was reversed overnight after addition of NaCl to a final concentration of 200 mM and 2 µg of proteinase K. DNA was purified with Qiaquick PCR purification columns (Qiagen) as indicated by the manufacturer.

For ChIP-qPCR, immunoprecipitated DNA was analyzed with SYBR-Green real-time qPCR using the standard-curve method, and quantity was expressed relative to input. ChIP-qPCR experiments were performed in triplicate. Primer sequences are listed in Table S2. For ChIP-seq, libraries were prepared using NEBNext Ultra II DNA Library Prep Kit for Illumina according to the manufacturer's instructions. NEBNext Multiplex Oligos for Illumina were used during library amplification. Single-ended sequencing was performed using the NextSeq 500/550 High-Output v2.5 (75 cycle) Kit (#20024906) on the NextSeq 550 platform at the Wellcome Trust Clinical Research Facility in Edinburgh, UK. ChIP-seq experiments were performed in duplicate.

Bioinformatics analysis

Read mapping and data visualization

ChIP-seq data generated here and publicly available raw datasets (ChIP seq and GRO-seq listed in Table S1) were aligned and processed as follows. Single-end ChIP-seq reads were mapped to the hg18 genome using Bowtie v1.0.0 (Langmead et al., 2009). Only sequences uniquely aligned with less than or equal to one mismatch were retained. The resulting files (.sam) were then converted into bam files using SAMtools (Li et al., 2009). Duplicated reads were removed using the SAMtools rmdup command (Li et al., 2009). For signal normalization and visualization on the University of California, Santa Cruz (UCSC) genome browser (Kent et al., 2002), the number of reads per kilobase per million mapped reads was counted using the bamCoverage command from deepTools (Ramírez et al., 2014), and BigWig files were generated. For Chip-seq datasets, reads were extended to 200 bp.

Peak calling

TF enrichment sites were detected with MACS2 version 2.1.1 (Zhang et al., 2008) using default parameters and a P value of 1e−5. A control dataset derived by sequencing input DNA samples was used to define a background model. For samples for which duplicate samples were available, we retained the peaks found in replicate experiments. We considered peaks to be overlapping if they shared a minimum of one base.

Motif discovery

De novo motif discovery was performed with HOMER (Heinz et al., 2010) using a window of 200 bp around the peak summits and setting motifs length to 8, 10, and 12 bp. The best scoring motif was chosen from each analysis to represent the DNA binding domain for each of the factors profiled. The coenriched motifs obtained for the different lengths were independently analyzed for consistency of results and manually curated to exclude redundant motifs. The top scoring motifs, ranked by P value, are shown in each case. Matching in vitro or in vivo DNA binding motifs were associated with the de novo recovered matrix when the HOMER score was 0.7 or higher.

Heat maps, average profiles, and differential binding analysis

Heat maps and average profiles for TF binding site midpoints were generated using deepTools (Ramírez et al., 2014). Differential binding analysis and related plots were performed as described previously (Stark and Brown, 2011). ChIP-seq read counts were TMM (trimmed mean of M values) normalized using full library size. GRO-seq read densities were analyzed in a manner similar to that of ChIP-Seq, and raw read counts from estradiol-treated samples were divided by the raw read count from the control-treated samples.

Subcellular fractionation and Western blotting

Subcellular fractionation was performed as previously described (Gagnon et al., 2014b). A pellet of ∼5–10 × 10^6 MCF-7 cells was washed in ice-cold PBS and resuspended in HLB buffer (10 mM Tris-HCl, pH 7.5, 10 mM NaCl, 3 mM $MgCl_2$, 0.3% Igepal CA630, 10% glycerol, and 1× protease inhibitors; Roche). 10-min incubation was performed in ice. Samples were centrifuged at 4°C and 800 *g* for 8 min. The pellet corresponds to intact nuclei and the supernatant to the cytoplasmatic fraction. Equal proportions of each fraction were analyzed by SDS-PAGE and transferred to nitrocellulose membranes (BioRad). Membranes were blocked with 5% milk and then incubated with the primary antibody. After washing, membranes were incubated with IR-Dye 800CW (LI-COR Biosciences) secondary antibodies. Bound antibody was detected using the Odyssey imaging system (LI-COR Biosciences).

Immunofluorescence

Cells were grown and treated on coverslips. They were fixed in 4% paraformaldehyde for 10 min and permeabilized in 1% Triton X-100 in PBS for another 10 min. Cells were blocked with 3% BSA in PBS for 30 min and further incubated with the primary antibody in a 1/1,000 dilution in blocking buffer for 1 h. Rat monoclonal anti-AGO1 antibody clone 4B8 was used. Cells were then incubated with the secondary antibody diluted 1/1,000 in 3% BSA PBS for 1 h. The secondary antibody used was the anti-goat anti-rat (Alexa Fluor 488; Abcam ab150157). Coverslips were washed with PBS for 5 min five times. Nuclei were stained with TOTO-3 iodide (Thermo Fisher Scientific). Images were taken with an Olympus FV1000 inverted confocal microscope using a 60× oil-immersion objective and FluoView Viewer software (Olympus). Images were further analyzed using CellProfiler software (Carpenter et al., 2006).

Coimmunoprecipitation assay

A pellet of ∼2 × 10^6 MCF-7 or HEK293 cells was lysed in 1 ml of lysis buffer (50 mM Tris-HCl, pH 7.5, 150 mM NaCl, 1 mM EDTA, 1% Igepal CA630, 0.5% sodium deoxycholate, 0.5 mM DTT, 1× protease inhibitors [Roche], 5 mM β-glycerophosphate, and 5 mM potassium fluoride) and incubated for 30 min at 4°C. After centrifugation for 20 min at 4°C, supernatants were immunoprecipitated overnight with 40 µl of protein G magnetic beads previously incubated with the antibody of interest for 1 h at 4°C. The following antibodies were used: 2 µg of rat monoclonal anti-AGO1 clone 4B8, 1 µg of rabbit polyclonal anti-ERα HC-20, and 2 µg of mouse monoclonal anti-FLAG clone M5 (Sigma-Aldrich). Control immunoprecipitations were performed with no antibody. Beads were washed four times with washing buffer (50 mM Tris-HCl, pH 7.5, 125 mM NaCl, 1 mM

EDTA, and 0.1% Igepal CA630) for 5 min at 4°C. Immunoprecipitate was eluted with 2× Laemmli sample buffer.

Expression analysis

RNA from MCF-7 cells grown in 12-well plates or MCF1 nuclei purified as explained before from 6-cm plates were isolated by using 500 µl of Tri-Reagent (MRC) following the manufacturer's instructions. 2 µg was reverse transcribed to cDNA with a random deca-oligonucleotide primer mix using MMLV Reverse transcription (Invitrogen). qPCRs were performed using SYBR Green dye and Taq DNA polymerase (Invitrogen). The annealing temperature was 60°C, and the elongation time at 72°C was 30 s. Relative RNA abundances from cDNAs and no-reverse transcription controls were estimated using internal standard curves with a PCR efficiency of 100 ± 10% for each set of primers in each experiment. Primer sequences are listed in Table S2.

3C

3C assay was performed as described before (Louwers et al., 2009; Naumova et al., 2012). 25 × 10^6 MCF-7 cells were fixed by adding 1% formaldehyde at room temperature for 10 min, and the reaction was stopped with 125 mM glycine. Lysis buffer (500 µl of 10 mM Tris-HCl, pH 8.0, 10 mM NaCl, 0.2% Igepal CA630, and 1× protease inhibitors) was added, and cells were incubated on ice 15 min. Next, cells were lysed with a Dounce homogenizer, and the suspension was spun down at 5,000 rpm at 4°C. The pellet was washed twice with 500 µl ice-cold 1× NEBuffer 2. The pellet was then resuspended in 1× NEBuffer 2 and split into five separate 50-µl aliquots. 362 µl of NEBuffer 2 was added to each aliquot. SDS was added to a 0.1% final concentration, and incubation at 65°C was performed for 10 min. Triton X-100 at a 1% final concentration was added, and nuclei were incubated at 37°C on a rotating wheel. Next, chromatin was digested overnight with 200 U NcoI (NEBuffer 2). On the next morning, 86 µl of 10% SDS was added to each tube, and they were incubated at 65°C for 10 min. Each digested chromatin mixture was ligated by 100 U T4 DNA Ligase (Promega) in 8 ml of Ligation Mix (1% Triton X-100, 1× Ligation Buffer, 1 mM ATP, and 0.1 mg/ml BSA) for 4 h at 16°C. The ligase step was omitted in one chromatin aliquot from the five mentioned above as the unligated control. The chromatin was subsequently de–cross-linked overnight at 65°C with 50 µg of proteinase A. DNA was purified twice with phenol and then with a mixture of phenol and chloroform (at a ratio of 1:1). DNA was precipitated, and pellets were air dried before resuspending in 250 µl 1× TE buffer. To degrade any carryover RNA, 1 µl RNase A was added to each tube and incubated at 37°C for 15 min. DNA was further purified using phenol/chloroform and then precipitated. The digestion and ligation efficiencies were checked and normalized before DNA analysis by SYBR-Green qPCR. Primer sequences are listed in Table S2.

Online supplemental material

Fig. S1 further supports our findings showing that AGO1 localizes at ERα binding sites in MCF-7 cells and that that AGO1 binding levels to chromatin increase with E2 treatment. It also shows ChIP-qPCR validation of AGO1 ChIP-seq findings. Fig. S2 shows both by subcellular fractionation followed by Western blot and by immunofluorescence that AGO1 nuclear relative to cytoplasmatic localization remains unchanged upon E2 treatment. Fig. S3 shows the enrichment levels of different chromatin states on ERα binding sites divided into $AGO1^+$ and $AGO1^-$. Fig. S3 further shows that ERα binding density is higher in AGO1 cobound regions. Additionally, it shows by ChIP-qPCR that AGO1 knockdown reduces its recruitment levels to chromatin and that AGO1 knockdown performed with two different siRNAs reduces the E2-dependent increase in mRNA levels (shown by RT-qPCR). Table S1 lists the citations corresponding to the published data used for the bioinformatic analysis. Table S2 lists the primer sequences used in this paper.

Acknowledgments

We thank Wendy Bickmore (Institute of Genetics and Molecular Medicine, University of Edinburgh, Edinburgh, UK) and Adalí Pecci (Universidad de Buenos Aires, Instituto de Fisiología, Biología Molecular y Neurociencias, Buenos Aires, Argentina) for useful discussions and reagents as well as members of the Kornblihtt and Srebrow laboratories for their invaluable help.

This work was supported by grants from the Agencia Nacional de Promoción Científica y Tecnológica of Argentina (PICT-2011 1617 and PICT-2014 2582), the Universidad de Buenos Aires (UBACYT 20020130100152BA), the International Research Scholar program of the Howard Hughes Medical Institute, and the Lounsbery Foundation. A.R. Kornblihtt, E. Nazer, and S.A. Rodríguez-Seguí are career investigators; V. Buggiano is a senior technician, and L.I. Gómez Acuña, B. Pozzi, and L.E. Marasco received fellowships from the Consejo Nacional de Investigaciones Científicas y Técnicas of Argentina.

The authors declare no competing financial interests.

Author contributions: L.I. Gómez Acuña and A.R. Kornblihtt conceived the project and designed the experiments. L.I. Gómez Acuña performed most of the experiments. S.A. Rodríguez-Seguí and L.I. Gómez Acuña performed the bioinformatic analysis. E. Nazer performed 3C and knockdown followed by rescue experiments. E. Nazer, B. Pozzi, V. Buggiano, L.E. Marasco, E. Agirre, and M. Alló participated in the execution of some of the experiments and participated with helpful discussions and ideas. L.I. Gómez Acuña and A.R. Kornblihtt wrote the manuscript. A.R. Kornblihtt supervised the project.

Submitted: 12 August 2019
Revised: 20 April 2020
Accepted: 20 May 2020

References

Ahlenstiel, C.L., H.G.W. Lim, D.A. Cooper, T. Ishida, A.D. Kelleher, and K. Suzuki. 2012. Direct evidence of nuclear Argonaute distribution during transcriptional silencing links the actin cytoskeleton to nuclear RNAi machinery in human cells. *Nucleic Acids Res.* 40:1579–1595. https://doi.org/10.1093/nar/gkr891

Alberts, B., A.D. Johnson, J. Lewis, D. Morgan, M. Raff, K. Roberts, and P. Walter. 2015. Molecular Biology of the Cell. Sixth edition. Garland Science, Taylor and Francis Group, New York.

Alló, M., V. Buggiano, J.P. Fededa, E. Petrillo, I. Schor, M. de la Mata, E. Agirre, M. Plass, E. Eyras, S.A. Elela, et al. 2009. Control of alternative splicing

through siRNA-mediated transcriptional gene silencing. *Nat. Struct. Mol. Biol.* 16:717–724. https://doi.org/10.1038/nsmb.1620

Alló, M., E. Agirre, S. Bessonov, P. Bertucci, L. Gómez Acuña, V. Buggiano, N. Bellora, B. Singh, E. Petrillo, M. Blaustein, et al. 2014. Argonaute-1 binds transcriptional enhancers and controls constitutive and alternative splicing in human cells. *Proc. Natl. Acad. Sci. USA.* 111:15622–15629. https://doi.org/10.1073/pnas.1416858111

Ameyar-Zazoua, M., C. Rachez, M. Souidi, P. Robin, L. Fritsch, R. Young, N. Morozova, R. Fenouil, N. Descostes, J.-C. Andrau, et al. 2012. Argonaute proteins couple chromatin silencing to alternative splicing. *Nat. Struct. Mol. Biol.* 19:998–1004. https://doi.org/10.1038/nsmb.2373

Burroughs, A.M., Y. Ando, M.J.L. de Hoon, Y. Tomaru, H. Suzuki, Y. Hayashizaki, and C.O. Daub. 2011. Deep-sequencing of human Argonaute-associated small RNAs provides insight into miRNA sorting and reveals Argonaute association with RNA fragments of diverse origin. *RNA Biol.* 8:158–177. https://doi.org/10.4161/rna.8.1.14300

Carpenter, A.E., T.R. Jones, M.R. Lamprecht, C. Clarke, I.H. Kang, O. Friman, D.A. Guertin, J.H. Chang, R.A. Lindquist, J. Moffat, et al. 2006. CellProfiler: image analysis software for identifying and quantifying cell phenotypes. *Genome Biol.* 7:R100. https://doi.org/10.1186/gb-2006-7-10-r100

Cernilogar, F.M., M.C. Onorati, G.O. Kothe, A.M. Burroughs, K.M. Parsi, A. Breiling, F. Lo Sardo, A. Saxena, K. Miyoshi, H. Siomi, et al. 2011. Chromatin-associated RNA interference components contribute to transcriptional regulation in Drosophila. *Nature.* 480:391–395. https://doi.org/10.1038/nature10492

Faehnle, C.R., E. Elkayam, A.D. Haase, G.J. Hannon, and L. Joshua-Tor. 2013. The making of a slicer: activation of human Argonaute-1. *Cell Rep.* 3: 1901–1909. https://doi.org/10.1016/j.celrep.2013.05.033

Gagnon, K.T., L. Li, Y. Chu, B.A. Janowski, and D.R. Corey. 2014a. RNAi Factors Are Present and Active in Human Cell Nuclei. *Cell Rep.* 6: 211–221. https://doi.org/10.1016/j.celrep.2013.12.013

Gagnon, K.T., L. Li, B.A. Janowski, and D.R. Corey. 2014b. Analysis of nuclear RNA interference in human cells by subcellular fractionation and Argonaute loading. *Nat. Protoc.* 9:2045–2060. https://doi.org/10.1038/nprot.2014.135

Gantier, M.P., and B.R.G. Williams. 2007. The response of mammalian cells to double-stranded RNA. *Cytokine Growth Factor Rev.* 18:363–371. https://doi.org/10.1016/j.cytogfr.2007.06.016

Guang, S., A.F. Bochner, K.B. Burkhart, N. Burton, D.M. Pavelec, and S. Kennedy. 2010. Small regulatory RNAs inhibit RNA polymerase II during the elongation phase of transcription. *Nature.* 465:1097–1101. https://doi.org/10.1038/nature09095

Guérin, T.M., F. Palladino, and V.J. Robert. 2014. Transgenerational functions of small RNA pathways in controlling gene expression in C. elegans. *Epigenetics.* 9:37–44. https://doi.org/10.4161/epi.26795

Hah, N., C.G. Danko, L. Core, J.J. Waterfall, A. Siepel, J.T. Lis, and W.L. Kraus. 2011. A rapid, extensive, and transient transcriptional response to estrogen signaling in breast cancer cells. *Cell.* 145:622–634. https://doi.org/10.1016/j.cell.2011.03.042

Hah, N., S. Murakami, A. Nagari, C.G. Danko, and W.L. Kraus. 2013. Enhancer transcripts mark active estrogen receptor binding sites. *Genome Res.* 23: 1210–1223. https://doi.org/10.1101/gr.152306.112

Han, J., D. Kim, and K.V. Morris. 2007. Promoter-associated RNA is required for RNA-directed transcriptional gene silencing in human cells. *Proc. Natl. Acad. Sci. USA.* 104:12422–12427. https://doi.org/10.1073/pnas.0701635104

Heinz, S., C. Benner, N. Spann, E. Bertolino, Y.C. Lin, P. Laslo, J.X. Cheng, C. Murre, H. Singh, and C.K. Glass. 2010. Simple combinations of lineage-determining transcription factors prime cis-regulatory elements required for macrophage and B cell identities. *Mol. Cell.* 38:576–589. https://doi.org/10.1016/j.molcel.2010.05.004

Holoch, D., and D. Moazed. 2015. RNA-mediated epigenetic regulation of gene expression. *Nat. Rev. Genet.* 16:71–84. https://doi.org/10.1038/nrg3863

Huang, V., J. Zheng, Z. Qi, J. Wang, R.F. Place, J. Yu, H. Li, and L.-C. Li. 2013. Ago1 Interacts with RNA polymerase II and binds to the promoters of actively transcribed genes in human cancer cells. *PLoS Genet.* 9. e1003821. https://doi.org/10.1371/journal.pgen.1003821

Hurtado, A., K.A. Holmes, C.S. Ross-Innes, D. Schmidt, and J.S. Carroll. 2011. FOXA1 is a key determinant of estrogen receptor function and endocrine response. *Nat. Genet.* 43:27–33. https://doi.org/10.1038/ng.730

Ipsaro, J.J., and L. Joshua-Tor. 2015. From guide to target: molecular insights into eukaryotic RNA-interference machinery. *Nat. Struct. Mol. Biol.* 22: 20–28. https://doi.org/10.1038/nsmb.2931

Janowski, B.A., K.E. Huffman, J.C. Schwartz, R. Ram, R. Nordsell, D.S. Shames, J.D. Minna, and D.R. Corey. 2006. Involvement of AGO1 and AGO2 in mammalian transcriptional silencing. *Nat. Struct. Mol. Biol.* 13: 787–792. https://doi.org/10.1038/nsmb1140

Janowski, B.A., S.T. Younger, D.B. Hardy, R. Ram, K.E. Huffman, and D.R. Corey. 2007. Activating gene expression in mammalian cells with promoter-targeted duplex RNAs. *Nat. Chem. Biol.* 3:166–173. https://doi.org/10.1038/nchembio860

Joshua-Tor, L., and G.J. Hannon. 2011. Ancestral roles of small RNAs: an Ago-centric perspective. *Cold Spring Harb. Perspect. Biol.* 3. a003772. https://doi.org/10.1101/cshperspect.a003772

Kent, W.J., C.W. Sugnet, T.S. Furey, K.M. Roskin, T.H. Pringle, A.M. Zahler, and D. Haussler. 2002. The human genome browser at UCSC. *Genome Res.* 12:996–1006. https://doi.org/10.1101/gr.229102

Langmead, B., C. Trapnell, M. Pop, and S.L. Salzberg. 2009. Ultrafast and memory-efficient alignment of short DNA sequences to the human genome. *Genome Biol.* 10:R25. https://doi.org/10.1186/gb-2009-10-3-r25

Le Romancer, M., C. Poulard, P. Cohen, S. Sentis, J.M. Renoir, and L. Corbo. 2011. Cracking the estrogen receptor's posttranslational code in breast tumors. *Endocr. Rev.* 32:597–622. https://doi.org/10.1210/er.2010-0016

Li, H., B. Handsaker, A. Wysoker, T. Fennell, J. Ruan, N. Homer, G. Marth, G. Abecasis, and R. Durbin; 1000 Genome Project Data Processing Subgroup. 2009. The Sequence Alignment/Map format and SAMtools. *Bioinformatics.* 25:2078–2079. https://doi.org/10.1093/bioinformatics/btp352

Li, W., D. Notani, Q. Ma, B. Tanasa, E. Nunez, A.Y. Chen, D. Merkurjev, J. Zhang, K. Ohgi, X. Song, et al. 2013. Functional roles of enhancer RNAs for oestrogen-dependent transcriptional activation. *Nature.* 498: 516–520. https://doi.org/10.1038/nature12210

Li, L., M. Matsui, and D.R. Corey. 2016. Activating frataxin expression by repeat-targeted nucleic acids. *Nat. Commun.* 7:10606. https://doi.org/10.1038/ncomms10606

Louwers, M., E. Splinter, R. van Driel, W. de Laat, and M. Stam. 2009. Studying physical chromatin interactions in plants using Chromosome Conformation Capture (3C). *Nat. Protoc.* 4:1216–1229. https://doi.org/10.1038/nprot.2009.113

Magnani, L., and M. Lupien. 2014. Chromatin and epigenetic determinants of estrogen receptor alpha (ESR1) signaling. *Mol. Cell. Endocrinol.* 382: 633–641. https://doi.org/10.1016/j.mce.2013.04.026

McKenna, N.J., and B.W. O'Malley. 2002. Combinatorial control of gene expression by nuclear receptors and coregulators. *Cell.* 108:465–474. https://doi.org/10.1016/S0092-8674(02)00641-4

Meister, G.. 2013. Argonaute proteins: functional insights and emerging roles. *Nat. Rev. Genet.* 14:447–459. https://doi.org/10.1038/nrg3462

Morris, K.V., S.W.-L. Chan, S.E. Jacobsen, and D.J. Looney. 2004. Small interfering RNA-induced transcriptional gene silencing in human cells. *Science.* 305:1289–1292. https://doi.org/10.1126/science.1101372

Moshkovich, N., P. Nisha, P.J. Boyle, B.A. Thompson, R.K. Dale, and E.P. Lei. 2011. RNAi-independent role for Argonaute2 in CTCF/CP190 chromatin insulator function. *Genes Dev.* 25:1686–1701. https://doi.org/10.1101/gad.16651211

Nacht, A.S., A. Pohl, R. Zaurin, D. Soronellas, J. Quilez, P. Sharma, R.H. Wright, M. Beato, and G.P. Vicent. 2016. Hormone-induced repression of genes requires BRG1-mediated H1.2 deposition at target promoters. *EMBO J.* 35:1822–1843. https://doi.org/10.15252/embj.201593260

Naumova, N., E.M. Smith, Y. Zhan, and J. Dekker. 2012. Analysis of long-range chromatin interactions using Chromosome Conformation Capture. *Methods.* 58:192–203. https://doi.org/10.1016/j.ymeth.2012.07.022

Nazer, E., R.K. Dale, M. Chinen, B. Radmanesh, and E.P. Lei. 2018a. Argonaute2 and LaminB modulate gene expression by controlling chromatin topology. *PLoS Genet.* 14:e1007276. https://doi.org/10.1371/journal.pgen.1007276

Nazer, E., R.K. Dale, C. Palmer, and E.P. Lei. 2018b. Argonaute2 attenuates active transcription by limiting RNA Polymerase II elongation in Drosophila melanogaster. *Sci. Rep.* 8:15685. https://doi.org/10.1038/s41598-018-34115-1

Ramírez, F., F. Dündar, S. Diehl, B.A. Grüning, and T. Manke. 2014. deepTools: a flexible platform for exploring deep-sequencing data. *Nucleic Acids Res.* 42(W1):W187–W191. https://doi.org/10.1093/nar/gku365

Renoir, J.-M.. 2012. Estradiol receptors in breast cancer cells: associated cofactors as targets for new therapeutic approaches. *Steroids.* 77:1249–1261. https://doi.org/10.1016/j.steroids.2012.07.019

Rüdel, S., Y. Wang, R. Lenobel, R. Körner, H.H. Hsiao, H. Urlaub, D. Patel, and G. Meister. 2011. Phosphorylation of human Argonaute proteins affects small RNA binding. *Nucleic Acids Res.* 39:2330–2343. https://doi.org/10.1093/nar/gkq1032

Shuaib, M., K.M. Parsi, M. Thimma, S.A. Adroub, H. Kawaji, L. Seridi, Y. Ghosheh, A. Fort, B. Fallatah, T. Ravasi, et al. 2019. Nuclear AGO1

Regulates Gene Expression by Affecting Chromatin Architecture in Human Cells. *Cell Syst*. 9:446–458.e6: E6. https://doi.org/10.1016/j.cels.2019.09.005

Stark, R., and G. Brown. 2011. *DiffBind*: Differential binding analysis of ChIP-Seq peak data. http://bioconductor.org/packages/release/bioc/vignettes/DiffBind/inst/doc/DiffBind.pdf.

Svoboda, P.. 2014. Renaissance of mammalian endogenous RNAi. *FEBS Lett*. 588:2550–2556. https://doi.org/10.1016/j.febslet.2014.05.030

Swarts, D.C., K. Makarova, Y. Wang, K. Nakanishi, R.F. Ketting, E.V. Koonin, D.J. Patel, and J. van der Oost. 2014. The evolutionary journey of Argonaute proteins. *Nat. Struct. Mol. Biol*. 21:743–753. https://doi.org/10.1038/nsmb.2879

Taberlay, P.C., A.L. Statham, T.K. Kelly, S.J. Clark, and P.A. Jones. 2014. Reconfiguration of nucleosome-depleted regions at distal regulatory elements accompanies DNA methylation of enhancers and insulators in cancer. *Genome Res*. 24:1421–1432. https://doi.org/10.1101/gr.163485.113

Taliaferro, J.M., J.L. Aspden, T. Bradley, D. Marwha, M. Blanchette, and D.C. Rio. 2013. Two new and distinct roles for Drosophila Argonaute-2 in the nucleus: alternative pre-mRNA splicing and transcriptional repression. *Genes Dev*. 27:378–389. https://doi.org/10.1101/gad.210708.112

Tam, O.H., A.A. Aravin, P. Stein, A. Girard, E.P. Murchison, S. Cheloufi, E. Hodges, M. Anger, R. Sachidanandam, R.M. Schultz, et al. 2008. Pseudogene-derived small interfering RNAs regulate gene expression in mouse oocytes. *Nature*. 453:534–538. https://doi.org/10.1038/nature06904

Tan, S.K., Z.H. Lin, C.W. Chang, V. Varang, K.R. Chng, Y.F. Pan, E.L. Yong, W.K. Sung, and E. Cheung. 2011. AP-2γ regulates oestrogen receptor-mediated long-range chromatin interaction and gene transcription. *EMBO J*. 30:2569–2581. https://doi.org/10.1038/emboj.2011.151

Tarallo, R., G. Giurato, G. Bruno, M. Ravo, F. Rizzo, A. Salvati, L. Ricciardi, G. Marchese, A. Cordella, T. Rocco, et al. 2017. The nuclear receptor ERβ engages AGO2 in regulation of gene transcription, RNA splicing and RISC loading. *Genome Biol*. 18:189. https://doi.org/10.1186/s13059-017-1321-0

Teytelman, L., D.M. Thurtle, J. Rine, and A. van Oudenaarden. 2013. Highly expressed loci are vulnerable to misleading ChIP localization of multiple unrelated proteins. *Proc. Natl. Acad. Sci. USA*. 110:18602–18607. https://doi.org/10.1073/pnas.1316064110

Vernimmen, D., and W.A. Bickmore. 2015. The Hierarchy of Transcriptional Activation: From Enhancer to Promoter. *Trends Genet*. 31:696–708. https://doi.org/10.1016/j.tig.2015.10.004

Xiao, R., J.Y. Chen, Z. Liang, D. Luo, G. Chen, Z.J. Lu, Y. Chen, B. Zhou, H. Li, X. Du, et al. 2019. Pervasive Chromatin-RNA Binding Protein Interactions Enable RNA-Based Regulation of Transcription. *Cell*. 178:107–121.e18. https://doi.org/10.1016/j.cell.2019.06.001

Yang, Y.H., S. Dudoit, P. Luu, D.M. Lin, V. Peng, J. Ngai, and T.P. Speed. 2002. Normalization for cDNA microarray data: a robust composite method addressing single and multiple slide systematic variation. *Nucleic Acids Res*. 30:e15. https://doi.org/10.1093/nar/30.4.e15

Zaytseva, O., N.C. Mitchell, L. Guo, O.J. Marshall, L.M. Parsons, R.D. Hannan, D.L. Levens, and L.M. Quinn. 2020. Transcriptional repression of Myc underlies AGO1's tumour suppressor function. *bioRxiv*. (Preprint posted March 11, 2020)https://doi.org/10.1101/2020.03.10.984906

Zhang, Y., T. Liu, C.A. Meyer, J. Eeckhoute, D.S. Johnson, B.E. Bernstein, C. Nusbaum, R.M. Myers, M. Brown, W. Li, et al. 2008. Model-based analysis of ChIP-Seq (MACS). *Genome Biol*. 9:R137. https://doi.org/10.1186/gb-2008-9-9-r137

Supplemental material

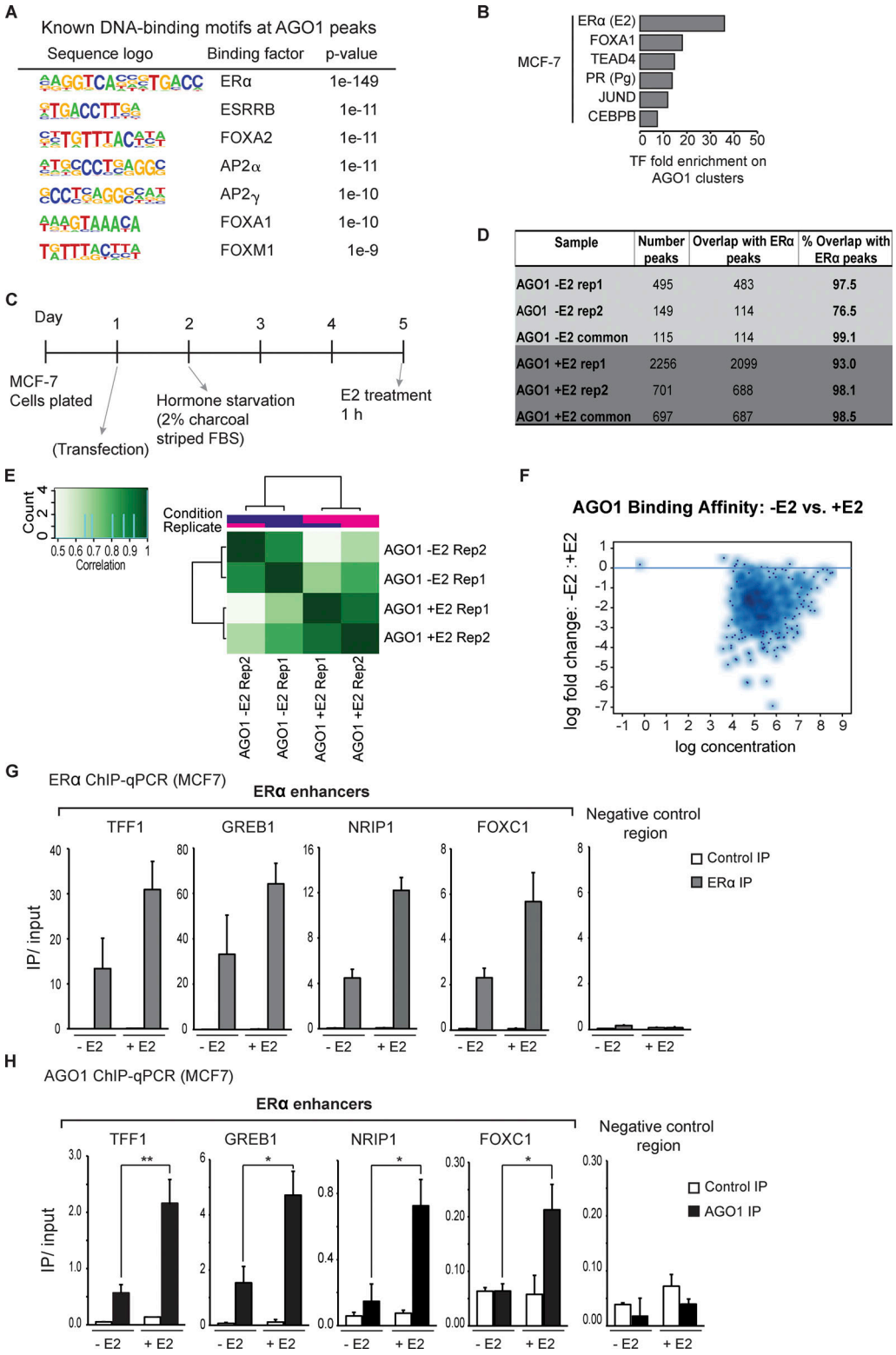

Figure S1. **Relative to Fig. 1: AGO1 locates at ERα binding sites, and its binding is enhanced by E2. (A)** Analysis of known DNA binding motifs of TFs expressed in MCF-7 cells at AGO1-associated genomic regions in serum-maintained cells. **(B)** Enrichment of TF binding at AGO1-associated regions in serum-maintained MCF7 cells. **(C)** Schematic representation of the hormone treatment experiments time line. **(D)** Table showing the overlap between the number of genomic sites (peaks) bound by ERα and by AGO1, considering each replicate separately and the common peaks. **(E)** Correlation heat map between AGO1 ChIP-seq samples and replicates based on read counts data on peak sets. **(F)** MA plot (gene expression ratios [Yang et al., 2002] depicting fold changes in AGO1 binding affinity between untreated and treated samples. **(G and H)** MCF-7 cells were hormone starved and then treated with vehicle or E2 for 1 h. **(G)** ERα binding to the enhancers was assessed by ChIP-qPCR. Data are represented as mean ± SD (n = 3). IP, immunoprecipitation. **(H)** AGO1 binding to the enhancers was assessed by ChIP-qPCR. Data are represented as mean ± SD (n = 3; *, P < 0.05; **, P < 0.01; two-tailed Student's t test).

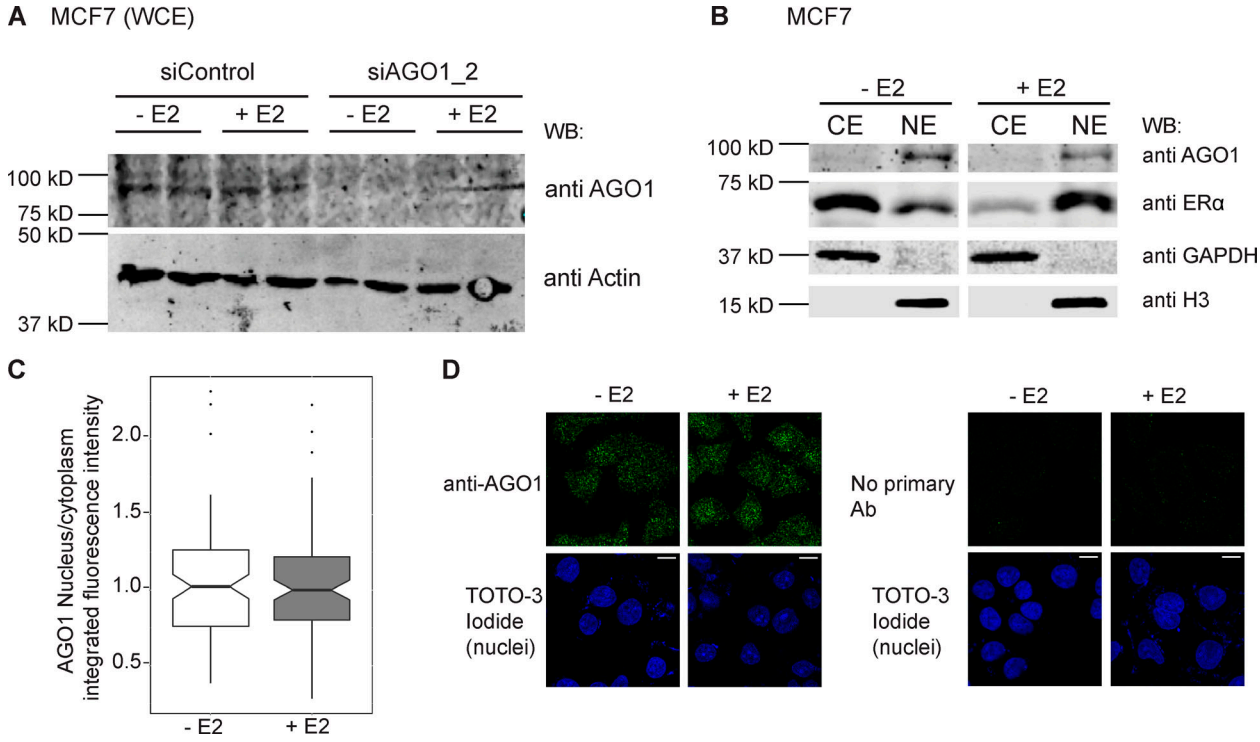

Figure S2. **AGO1 locates at ERα binding sites, and its binding is enhanced by E2 without changes in its subcellular localization. (A–D)** MCF-7 cells were hormone starved and then treated with vehicle or E2 for 1 h. **(A)** AGO1 levels in starved (−E2) and E2-treated (+E2) cells were tested by Western blot (WB) from whole-cell extracts (WCE; lanes 1–4). AGO1 levels were also assessed under these same conditions but transfected with a specific siRNA against AGO1 (lanes 5–8). **(B)** AGO1 and levels were assessed by Western blot in nuclear (NE) and cytoplasmic extracts (CE) from starved (−E2) and E2-treated MCF-7 cells. **(C)** AGO1 subcellular localization was assessed by immunofluorescence followed by confocal microscopy. The box plot corresponds to nucleus/cytoplasm integrated intensity ratios (n = 100 cells; two-tailed Student's t test). **(D)** Panels show representative images from C. Scale bars represent 10 µm.

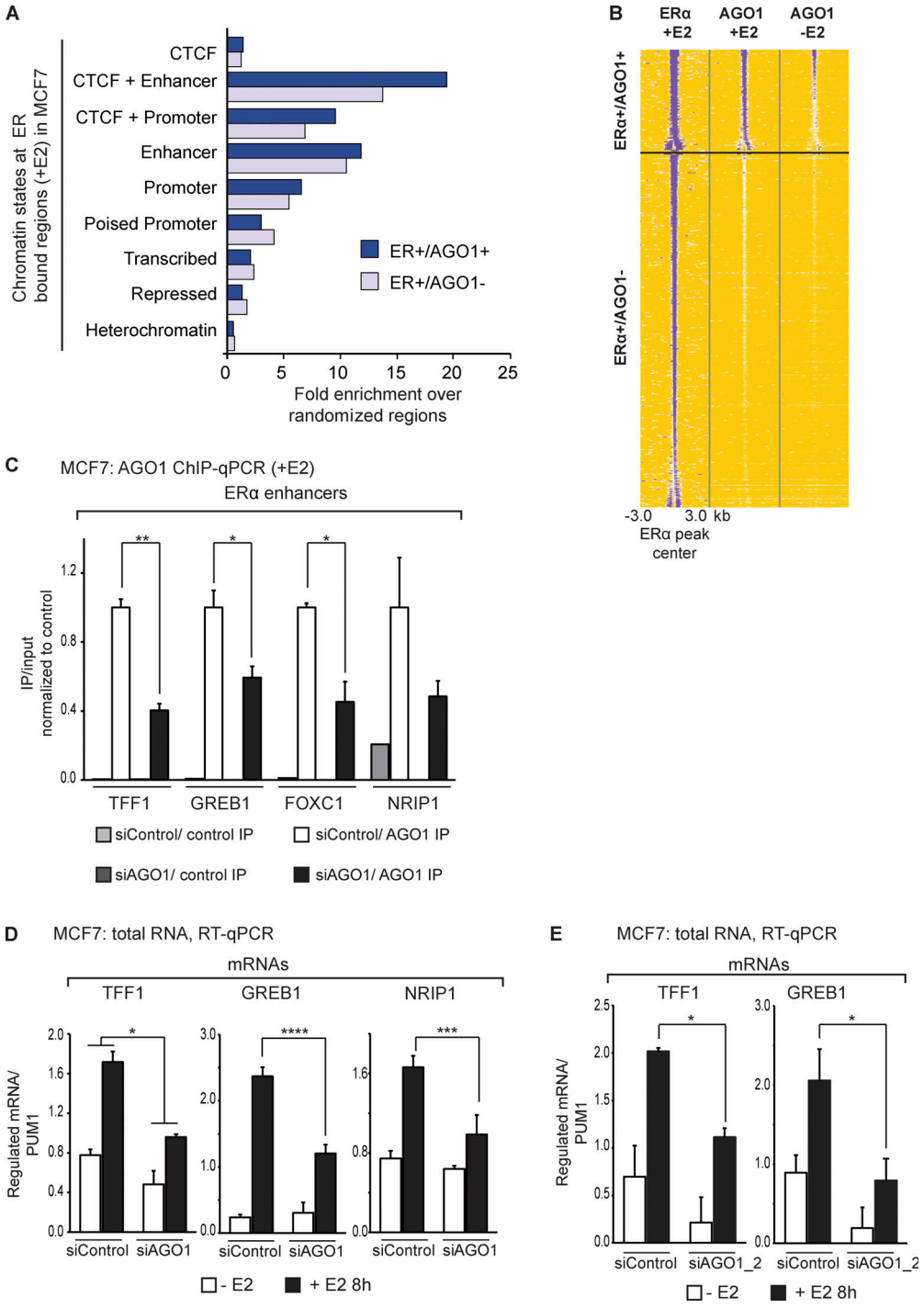

Figure S3. **Relative to Figs. 2 and 4. ERα binding intensity positively correlates with AGO1 binding, and AGO1 participates in the transcriptional activation of E2-responsive genes controlled by ERα enhancers. (A)** Enrichment of the indicated chromatin states, obtained from E2-treated MCF-7 cells, over ERα binding sites divided into ERα$^+$/AGO1$^+$ and ERα$^+$/AGO1$^-$. **(B)**. Heat maps of ChIP-seq signal centered (±3 kb) on ERα binding site midpoints for ERα (+E2), AGO1 (−E2), and AGO1 (+E2). ERα regions were divided according to whether they overlap with AGO1 (ERα$^+$/AGO1$^+$) or not (ERα$^+$/AGO1$^-$), and within each group, they were ordered from high to low ERα signal. **(C–E)** MCF-7 cells were transfected with an siControl or siAGO1. 24 h later, they were hormone starved, and 72 h later, they were treated with E2 or vehicle for the indicated time. **(C)** E2-dependent AGO1 recruitment to the enhancers upon AGO1 knockdown was controlled by ChIP-qPCR. Data are represented as mean ± SD (n = 3; *, P < 0.05; **, P < 0.01; two-tailed Student's t test). **(D)** RNA was extracted, and the indicated mRNA levels were analyzed by RT-qPCR. **(E)** Same as D, but a different siRNA against AGO1 was used. Values in D and E represent mean ± SE from three independent experiments (*, P < 0.05; **, P < 0.01; ***, P < 0.001; ****, P < 0.0001; ANOVA and Tukey post-hoc test). In A and B, two different siRNAs against AGO1 were used.

Provided online are two tables. Table S1 lists datasets used in the bioinformatic analysis, and Table S2 lists the oligonucleotides used in this study.